Phosphoprotein Phosphatase Activity Positively Regulates Oligomeric Pyrin to Trigger Inflammasome Assembly in Response to Bacterial Effectors and Toxins that Inactivate RhoA in Macrophages

Haleema S. Malik[1], Nicole A. Loeven[1], Jose M. Delgado[2], Arminja N. Kettenbach[1,2] and James B. Bliska[1]

[1]Department of Microbiology and Immunology, and [2]Department of Biochemistry and Cell Biology, Geisel School of Medicine at Dartmouth, Hanover NH, USA

[2]Norris Cotton Cancer Center, Lebanon, NH, USA.

Correspondence:
James B. Bliska
Department of Microbiology and Immunology, Geisel School of Medicine at Dartmouth, 66 College Street, Hanover NH, 03755 USA
Email: james.bliska@dartmouth.edu

ABSTRACT:

Pyrin is a pattern-recognition receptor in phagocytes that triggers capase-1 inflammasome assembly in response to bacterial toxins and effectors that inactivate RhoA. Pyrin contains coiled coil and B-box domains that promote oligomerization. Pyrin is negatively regulated by phosphorylation of two linker domain residues, S205 and S241 (murine) or S208 and S242 (human), via the kinase PKN, which is in turn activated by RhoA. Inactivation of RhoA by the TcdB toxin of *Clostridioides difficile*, the YopE and YopT effectors of *Yersinia,* or the TecA effector of *Burkholderia cenocepacia* triggers pyrin inflammasome assembly in macrophages. Inactivation of RhoA removes the negative regulation but a phosphoprotein phosphatase (PPP) is needed to positively regulate pyrin by dephosphorylation. No PPP that dephosphorylates pyrin has been identified, the oligomeric state of murine pyrin has not been determined, and the phosphorylation status of pyrin oligomers is unknown. We used primary murine macrophages and human THP-1 cells combined with the use of inhibitors, native PAGE, immunoblotting with phospho-specific pyrin antibodies and siRNA knockdowns to determine if a PPP positively regulates oligomeric pyrin. Results obtained with inhibitor calyculin A indicate that PPP activity is required to dephosphorylate S205 or S242 in murine or human pyrin, respectively, in response to inactivation of RhoA by TcdB, YopE/T or TecA. Findings from native PAGE show that murine pyrin exists as dimers and higher order oligomers that are phosphorylated on S205 prior to RhoA inactivation. Calyculin A treatment causes reduced mobility of murine pyrin on native PAGE and hyperphosphorylation of S242 in human pyrin, suggesting a PPP constitutively counterbalances PKN to keep the second linker site hypophosphorylated. Data from low dose okadaic acid and siRNA knockdown experiments implicates PP2A in dephosphorylation of S205 and positive regulation of pyrin in response to RhoA inactivation.

50 INTRODUCTION

51 Numerous Gram-negative bacterial pathogens encode type III secretion systems (T3SSs) that
52 are essential for virulence (1). T3SSs translocate effectors into or across the plasma membrane
53 and into the eukaryotic cytosol during bacterial-host cell contact. Translocated effectors can inhibit
54 innate immune responses to promote pathogenesis (1, 2). Host cells can sense perturbations
55 caused by T3SSs and/or effectors and produce compensatory innate immune responses to
56 counteract infection by pathogens (3, 4). Perturbations induced by T3SSs and/or effectors in
57 macrophages infected with bacterial pathogens can result in the assembly of caspase-1
58 inflammasomes (5, 6). Inflammasomes are multi-oligomeric complexes that are assembled in
59 response to various danger signals in the cell cytosol and serve as a molecular platform for the
60 recruitment and maturation of caspase-1 into its active form (5, 6). Active caspase-1 cleaves
61 gasdermin-D (GSDMD), pro-IL-1β and pro-IL-18 (7-9). The N-terminal domain of GSDMD forms
62 pores in the plasma membrane which allow for release of mature IL-1β and IL-18 (7-9). GSDMD
63 pores can also promote cell death, termed pyroptosis, resulting in the release of additional pro-
64 inflammatory molecules and intracellular bacteria (10). Pyroptosis amplifies the immune response
65 by restricting growth of bacteria and facilitating bacterial clearance by neutrophils (7). Virulent
66 bacterial pathogens can inhibit caspase-1 inflammasomes in host cells to counteract protective
67 immune responses mediated by IL-1β, IL-18 and pyroptosis (11).

68 *Yersinia* species are Gram-negative bacterial pathogens that cause invasive human infections
69 ranging in severity from plague (*Y. pestis*) to mesenteric lymphadenitis (*Y. pseudotuberculosis,*
70 *Yptb*). These bacteria replicate in lymphoid tissues as extracellular microcolonies and require a
71 plasmid-encoded T3SS for virulence (12). The T3SS delivers seven effectors called *Yersinia* outer
72 proteins (Yops) into the cytosol of phagocytes that are in contact with *Yersinia* (12). The effectors
73 inhibit key host cell processes, including phagocytosis and proinflammatory cytokine production
74 (13). For example, YopE and YopT inhibit phagocytosis by inactivating Rho GTPases, including
75 RhoA (13). YopE mimics a Rho GTPase activating protein (GAP) to accelerate GTP hydrolysis to
76 GDP in RhoA (14), while YopT is a cysteine protease which cleaves RhoA at its C-terminus so
77 that it is released from the membrane (15). Two effectors that are essential virulence factors inhibit
78 inflammasome activation: YopM, a leucine-rich repeat (LRR)-containing protein (16-18) and YopK
79 (19, 20). YopM inhibits the pyrin inflammasome (17, 18). YopK interacts with *Yersinia* translocon
80 components to limit activation of NLRP3 and NLRC4 inflammasomes (19).

81 Inactivation of RhoA by YopE or YopT in macrophages triggers assembly of the pyrin
82 inflammasome as a compensatory protective innate immune response (17, 18, 21, 22). Pyrin is a
83 cytosolic pattern recognition receptor (PRR) which specifically senses pathogen induced
84 modifications to RhoA (or RhoB or RhoC) to assemble an inflammasome (23). RhoA, RhoB and
85 RhoC appear to be functionally redundant in regulating pyrin activity (23) and will be referred to
86 as RhoA from here on. Inactivation of RhoA by the TcdB toxin of *Clostridioides difficile* or the
87 TecA effector of *Burkholderia cenocepacia* also triggers pyrin inflammasome assembly in
88 macrophages (23, 24). Pyrin is encoded by the *MEFV* gene (*Mefv* in mice) whose expression is
89 restricted to phagocytes such as neutrophils, monocytes and activated macrophages (25). Pyrin
90 is a TRIM protein and like other members of this family (26) human pyrin forms dimers via coiled
91 coil (CC) domains (27). Additionally, human pyrin has been shown to form trimers (28). Pyrin
92 potentially forms higher order oligomers (i.e. dimers of dimers), via B-box domains (21). It is not
93 known if murine pyrin forms oligomers. Structurally, murine and human pyrin are similar except
94 for their C-terminus. Murine pyrin lacks the B30.2 domain present in human pyrin (29). However,
95 the mechanism of pyrin regulation appears to be conserved in both species (30).

96 Negative regulation of pyrin occurs in a manner similar to the guard hypothesis observed in plants,
97 whereby a plant disease resistance PRR recognizes modifications to host proteins made by
98 pathogens and induces an innate response (31). More specifically, pyrin follows an indirect guard
99 hypothesis in which it does not directly interact with but is negatively regulated by RhoA (23).
100 Hence, pyrin acts as the guard of RhoA (guardee) to protect host cells from bacterial effectors or
101 toxins which target it. RhoA functions through a switch like mechanism between an “on” (Rho-
102 GTP) and “off” (Rho-GDP) state. RhoA has numerous roles in phagocytosis, cell cycle and
103 migration and is targeted by multiple bacterial pathogens (23, 32). Pyrin is negatively regulated
104 by serine phosphorylation, via the kinase PKN (also known as PRK), which is in turn is activated
105 by RhoA. PKN phosphorylates murine pyrin on serines 205 and 241 (S208 and S242 in human
106 pyrin) within 14-3-3-binding sites located in the linker region to negatively regulate pyrin (30, 33).
107 Mutational analysis of S205 and S241 by alanine substitution in ectopically expressed murine
108 pyrin indicates that loss of either site results in partial inflammasome activation and when both
109 sites are disrupted there is an additive effect (30). Similar studies of S208 and S242 in human
110 pyrin show that the inflammasome is activated when either site is substituted (33, 34). Moreover,
111 an S242R mutation in MEFV causes an autoinflammatory disease, PAAND, which leads to a
112 partially active form of pyrin and further underscores the importance of linker phosphorylation in
113 pyrin regulation (35). When pyrin is phosphorylated, the N-terminal pyrin domain (PYD) may be

114 sequestered, preventing interaction with ASC (21). RhoA inactivation removes the negative
115 regulation axis of pyrin, presumably resulting in dephosphorylation of S205/S208 and S241/S242
116 (21, 22, 30, 33). These findings lead to a model wherein when both serines in the pyrin linker are
117 dephosphorylated, 14-3-3 detaches, the PYD is exposed, and ASC and caspase-1 are recruited
118 to assemble inflammasomes (21, 30, 33). A limitation of this model is that no phosphoprotein
119 phosphatase (PPP) that dephosphorylates pyrin has been identified and the phosphorylation
120 status of pyrin oligomers is unknown.

121 Assembly of the pyrin inflammasome in phagocytes infected with WT *Yersinia* is blocked due to
122 the action of YopM (17, 18). YopM binds to and activates the protein PKN and a second kinase,
123 RSK (36). YopM hijacks PKN and RSK to keep pyrin phosphorylated (17, 21, 34). A *Yptb* Δ*yopM*
124 mutant is fully virulent in Mefv$^{-/-}$ mice, demonstrating that YopM promotes virulence by inhibiting
125 pyrin (17). The importance of pyrin in pathogenesis extends beyond *Yersinia, C. difficile* and *B.*
126 *cenocepacia* as numerous other bacteria including *Clostridium botulinum*, *Vibrio*
127 *parahaemolyticus* and *Histophilus somni* secrete toxins that trigger assembly of this
128 inflammasome in phagocytes (23).

129 Codon changes in the *MEFV* gene that result in gain of function pyrin variants are responsible for
130 the monogenic human autoinflammatory disease Familial Mediterranean Fever (FMF) (25, 34).
131 FMF is characterized by recurrent episodes of fever and serositis and primarily effects eastern
132 Mediterranean populations (37). Magnotti et al demonstrated that pyrin dephosphorylation was
133 sufficient to promote inflammasome activation using PKN inhibitors on monocytes from FMF
134 patients, which implies that these patients have a lower threshold for pyrin activation than healthy
135 patients (38). It has been hypothesized that the high carrier frequency of FMF in Mediterranean
136 and Middle Eastern populations is the result of a selective advantage in resistance to an unknown
137 infection (34). Population genetic evidence is consistent with the idea that plague selected for
138 FMF mutations in Middle Eastern populations (34). In addition, infection assays with human cells
139 and mice provided evidence that pyrin FMF variants promote resistance to *Y. pestis* (34). These
140 finding underscore the importance of the pyrin inflammasome for human health. Therefore, it is
141 important to understand the dual role of pyrin in promoting immune responses against pathogens
142 and FMF and a deeper understanding of pyrin inflammasome regulation will aid in this goal.

143 Here we used primary murine macrophages and human THP-1 cells in conjunction with PPP
144 inhibitors, native PAGE, immunoblotting with phospho-specific pyrin antibodies and siRNA
145 knockdowns to determine if PPP activity is required to dephosphorylate oligomeric pyrin and

146 positively regulate inflammasome assembly in response to bacterial effectors and toxins (YopE,
147 YopT, TecA or TcdB) that inactivate RhoA.
148
149 RESULTS
150 **PPP activity is required for pyrin dephosphorylation and positive regulation of**
151 **inflammasome assembly**
152 Inactivation of RhoA removes negative regulation by PKN, however, a PPP is needed to positively
153 regulate pyrin by serine dephosphorylation. The PPP family consists of PP1, PP2A, PP2B (also
154 known as calcineurin or PP3), PP4, PP5, PP6, and PP7 (39). To test the role of PPPs in
155 dephosphorylation of pyrin LPS-primed bone marrow-derived macrophages (BMDMs) were
156 pretreated for 15 min with DMSO as a vehicle control or one the following inhibitors: calyculin A
157 (CA) at 10 nM and okadaic acid (OA) at 1000 nM, which at these concentrations inhibit PP1,
158 PP2A, PP4, PP5, and PP6 but not PP2B; OA at 100 nM to more specifically inhibit PP2A; and
159 1000nM of cyclosporin A (CSA) which inhibits PP2B. After the pretreatment the BMDMs were
160 maintained in the presence of DMSO or the inhibitors during intoxication for 90 min with *C. difficile*
161 TcdB, which glucosylates and inactivates RhoA (40), to trigger pyrin inflammasome assembly
162 (23). BMDM lysates were analyzed by immunoblotting with commercially available monoclonal
163 antibodies specific for total pyrin or phosphoserine 205 (PS205) (30) or actin as loading control.
164 We were unable to monitor PS241 in murine pyrin because the antibody reported to recognize
165 this modification (30) did not work in our hands for this purpose but did recognize human pyrin
166 PS242 (see Fig.S3 below). We found that treatment of BMDMs with CA or 1000 nM OA prevented
167 pyrin S205 dephosphorylation in response to TcdB intoxication (Fig. S1A). Results of ELISA on
168 BMDM supernatants showed that CA or 1000 nM OA also significantly reduced release of mature
169 IL-1β during TcdB intoxication (Fig. S1B). CSA treatment did not inhibit pyrin S205
170 dephosphorylation or IL-1β release upon TcdB intoxication (Fig.S1) which indicates that PP2B
171 does not regulate this inflammasome. 100nM OA treatment was also ineffective (Fig. S1) but
172 previous publications (41) and subsequent experiments (see Fig. 4 below) indicate that at this
173 concentration longer pretreatments are needed for the inhibitor to reach effective concentrations
174 in cells. We noted that CA and 1000nM OA in the absence or presence of TcdB caused an upshift
175 in the positions of pyrin bands on the immunoblots, but not a corresponding increase in PS205
176 signal (Fig.S1A). This observation suggests that S205 is uniformly phosphorylated and a PPP
177 constitutively dephosphorylates pyrin at an additional site(s), possibly S241, and when this
178 phosphatase is inhibited, hyperphosphorylation by PKN results in reduced mobility of pyrin by
179 SDS-PAGE. In summary, these results suggest that a PPP other than PP2B is required to

180 dephosphorylate pyrin S205 and trigger assembly of the inflammasome in response to TcdB. In
181 addition, a PPP may act constitutively to dephosphorylate pyrin at another site(s).

182 We used CA treatment to determine if a PPP is important for YopE and YopT to trigger pyrin S205
183 dephosphorylation and inflammasome assembly in BMDMs infected with *Yptb.* BMDMs treated
184 with DMSO or CA as above were infected with a Δ*yopM* mutant to activate the pyrin
185 inflammasome. We also infected DMSO or CA-treated BMDMs with a Δ*yopK* mutant, which
186 triggers assembly of the NLRP3 inflammasome (and to a lesser degree the NLRC4
187 inflammasome) (19, 20), since there is evidence that PP2A is important for dephosphorylation
188 and activation of NLRP3 (42). Immunoblot and ELISA analysis of BMDMs pre-treated with CA
189 followed by Δ*yopM* infection showed that pyrin remained phosphorylated on S205 and there was
190 a significant decrease in IL-1β release (Fig. 1). Results of infection with Δ*yopK* also showed
191 reduced IL-1β release when the BMDMs were treated with CA, although the decrease was not
192 significant (Fig. 1B). Pyrin was not dephosphorylated on S205 in response to Δ*yopK* infection of
193 untreated BMDMs as expected (Fig. 1A). The finding that CA had a stronger inhibitory effect on
194 IL-1β secretion with Δ*yopM* as compared to Δ*yopK* infection (Fig. 1B) might reflect residual
195 NLRC4 inflammasome assembly triggered by the latter strain (19).

196 Similar results were obtained when CA was used to treat BMDMs infected with Δ*yopM Yptb*
197 strains expressing only active YopE ($yopT^{C139A}$) or YopT ($yopE^{R144A}$) (Fig. S2). In addition,
198 immunoblotting indicated that CA did not decrease steady state levels of pro-IL-1β (Fig. S2A).
199
200 *B. cenocepacia* infection of naive THP-1 cells has been shown to trigger assembly of the pyrin
201 inflammasome (43). To determine if PPP inhibition prevents dephosphorylation of human pyrin
202 we infected THP-1 cells with *B. cenocepacia* WT or Δ*tecA* strains in the absence or presence of
203 DMSO or CA. Lysates were immunoblotted with antibodies that recognize total pyrin, PS242,
204 pro-IL-1β or actin as loading control. *B. cenocepacia* infection triggered dephosphorylation of
205 S242 in a TecA-dependent manner in DMSO-treated THP-1 cells (Fig.S3). Interestingly, when
206 THP-1 cells were pretreated and maintained in the presence of CA S242 became
207 hyperphosphorylated in both uninfected and infected conditions (Fig.S3), which was evident from
208 comparing the short and long exposures of the immunoblots. The hyperphosphorylation of pyrin
209 in the presence of CA in uninfected THP-1 cells suggests that a PPP is constitutively
210 counterbalancing PKN to keep S242 hypophosphorylated. CA treatment prevented infection-
211 induced production of pro-IL-1β as determined by immunoblotting (Fig.S3) and as a result the

212 impact of the inhibitor on release of mature IL-1β from the THP-1 cells could not be measured.
213 These data indicate that a PPP dephosphorylates pyrin S242 in response to inactivation of RhoA
214 by TecA in THP-1 cells, however, it also appears that a PPP is acting constitutively to keep most
215 of the pyrin in the cell dephosphorylated at this site prior to infection.
216
217 **PPP activity regulates phosphorylation of oligomeric pyrin**
218 Although human pyrin has been shown to form trimers (28) the oligomeric status of murine pyrin
219 has not been investigated. In addition, it is not known if pyrin oligomers are differentially
220 phosphorylated or dephosphorylated. We used blue native PAGE (BN-PAGE) and
221 immunoblotting (44, 45) to examine the impact RhoA inactivation and PPP inhibition on
222 phosphorylation of oligomeric pyrin. To optimize the procedure, we first tested different non-ionic
223 detergent extraction conditions on untreated uninfected WT or *Mefv*$^{-/-}$ BMDMs. As shown in
224 Fig.S4, when extracts of untreated BMDMs were separated by BN-PAGE and immunoblotted for
225 total (A) or PS205 (B) pyrin, we detected oligomers of pyrin in WT but not *Mefv*$^{-/-}$ BMDMs.
226 Monomeric pyrin (~90 kDa) was not detected and based on the apparent molecular weight of the
227 oligomers we tentatively assigned them as dimer (~242 kDa) and higher-order oligomers (~480-
228 720 kDa). Thus, most of the pyrin in BMDMs is in a higher oligomeric form and phosphorylated
229 on S205. Recovery of total and PS205 pyrin was optimal using 0.5% or 1% digitonin (Fig.S4) and
230 1% was used going forward.
231
232 We next analyzed the phosphorylation and oligomeric status of pyrin in BMDMS infected with WT
233 or Δ*yopM Yptb* in the absence of CA using BN-PAGE and immunoblotting. As shown in Fig.2, the
234 total (A) and PS205 (B) pyrin oligomer signals decreased in BMDMs infected with Δ*yopM*, due
235 increased insolubility of the dephosphorylated form of pyrin in non-ionic detergent (E) (22). This
236 insolubility issue prevented us from determining if the oligomeric state of pyrin is altered upon
237 dephosphorylation. In BMDMs treated with CA there was an upshift in the positions of the dimeric
238 and higher oligomeric forms under all conditions, most evident with the PS205 signal, and there
239 was no insolubility or dephosphorylation of pyrin in response to infection with Δ*yopM* (Fig.2CD).
240 In addition, in the presence of CA a very large mystery oligomer at ~1048 kDa was detected with
241 the PS205 signal under all conditions (Fig.2D). These results confirm the upshift in mobility due
242 to hyperphosphorylation of pyrin in the presence of CA seen in some SDS-PAGE immunoblots
243 (Fig.S1A). These data further suggest that hyperphosphorylation of pyrin increases
244 oligomerization.
245

246 **YopM interacts with oligomeric pyrin**

247 YopM can interact with pyrin as determined by co-immunoprecipitation (17, 18, 34). We
248 wondered if YopM interacts with the different oligomeric forms of YopM and if this interaction is
249 sensitive to PPP inhibition. To determine if YopM is associated with pyrin oligomers, samples
250 from untreated WT BMDMs left uninfected or infected with WT or Δ*yopM Yptb* were separated by
251 BN-PAGE and immunoblotted with antibody to YopM. We detected a YopM signal at the dimer
252 and higher-order oligomer positions in the WT but not in the Δ*yopM Yptb* samples (Fig.3A, lanes
253 2 and 3). We then repeated the experiments using WT BMDMs untreated or treated with CA or
254 untreated *Mefv*$^{-/-}$ BMDMs. In WT BMDMs there was a YopM signal corresponding to dimeric pyrin
255 in the DMSO and CA treated WT *Yptb* infected samples (Fig.3B, lanes 2 and 5). The higher order
256 oligomeric YopM signal around ~480kDa seen with DMSO treatment was not present in the CA
257 treated sample (Fig.3B, lane 5). In addition, there was a faint YopM signal around ~480kDa in
258 the *Mefv*$^{-/-}$ BMDMs infected with WT *Yptb* (Fig.3B, lane 8). Two dimensional BN-PAGE
259 immunoblot analysis of the DMSO treated and WT *Yptb* infected BMDMs sample showed a good
260 correspondence in the molecular weights of the YopM and oligomeric pyrin signals (Fig. 3C).
261 These results strongly indicate that YopM interacts with dimeric and higher order oligomers of
262 pyrin. Possible explanations for why YopM interaction with the higher order pyrin oligomer is
263 sensitive to PPP inhibition, and the presence of a weak YopM signal at this position in Mefv-/-
264 BMDMs are discussed below (see Discussion).

265

266 **The PP1 inhibitor tautomycetin does not prevent pyrin dephosphorylation or**
267 **inflammasome assembly**

268 To further delineate which PPP activities positively regulate pyrin, we used tautomycetin (TTN),
269 a more specific inhibitor of PP1 (46, 47). WT BMDMs were pretreated for 15 min and maintained
270 in DMSO or 1 or 2μM of TTN during infection with Δ*yopM Yptb.* We found that treatment of
271 BMDMs with TTN did not prevent pyrin PS205 dephosphorylation or IL-1β release in response to
272 infection with Δ*yopM Yptb* (Fig.S4). Longer pretreatment of BMDMs with 1μM TTN also did not
273 decrease IL-1β secretion upon Δ*yopM* infection (data not shown). Our combined results from
274 treatment of BMDMs with various phosphatase inhibitors suggest that a PPP other than PP1 and
275 PP2B is required to activate pyrin.

276

277 **Longer pretreatment with 100 nM OA reduces pyrin dephosphorylation and inflammasome**
278 **assembly**

279 As mentioned previously, OA penetration inside cells is slow and using a lower concentration of
280 OA generally requires longer pretreatment time to achieve sufficient inhibitory levels inside the
281 cell. In contrast CA readily partitions inside cells (41, 48, 49). We found that WT BMDMs
282 pretreated for 3 hrs and maintained with 100nM OA during infection with Δ*yopM Yptb* showed
283 reduced pyrin dephosphorylation (Fig. 4A) and a significant decrease in IL-1β release as
284 compared to the DMSO control (Fig.4B); whereas 15min pretreatment of BMDMs with 100nM OA
285 did not have such an inhibitory effect on pyrin activation (Fig. S1). Given the selectivity of 100 nM
286 OA to preferentially inhibit PP2A/PP4 over PP1/PP5 (49), these results suggest that PP2A or PP4
287 could be involved in positively regulating pyrin. Since most serine/threonine phosphatase
288 activities inside the cell are carried out PP1 and PP2A (39, 50) our results with TTN and longer
289 pretreatment with OA in BMDMs allude to a role for PP2A in positive regulation of pyrin activation.
290

291 **siRNA knockdown implicates PP2A in dephosphorylation of pyrin S205**

292 We next tested the effect of knocking down PP2A in BMDMs on pyrin inflammasome assembly.
293 PP2A has two catalytic subunit isoforms, alpha (PP2Aca) and beta (PP2Acb), which only differ in
294 a few amino acids from each other. We first tested two different siRNAs targeting the mRNA of
295 the alpha catalytic subunit of PP2A (42). The siRNAs (1000pmol) were electroporated into WT
296 BMDMs which were also LPS-primed. PKN1 siRNA was used as a positive control (17, 33). RT-
297 qPCR showed that there was significant and selective knock down of PP2Aca mRNA with both
298 siRNAs as compared to the positive control and PP2Acb analyzed in parallel (Fig. 5A). The siRNA
299 electroporations were then repeated and LPS-primed BMDMs were left uninfected or infected
300 with Δ*yopM Yptb.* Immunoblotting showed that there was full depletion of PKN1 with the
301 corresponding siRNA but only an apparent ~50% knock down of PP2A with the siRNAs #1 and
302 #2 (Fig.5B). However, since the PP2A antibody used detects both isoforms the remaining signal
303 detected could have corresponded to PP2Acb. Upon Δ*yopM* infection there was no inhibition of
304 dephosphorylation of pyrin at S205 with either PP2Aca siRNAs (Fig. 5B). We next tested the
305 effect of a combined PP2A alpha and beta catalytic subunit knock down. BMDMs were
306 electroporated with PKN1 or PP2Aca #2 siRNA and PP2Acb #1 siRNA (500pmol each) and LPS
307 primed as before. RT-qPCR showed that there was a decrease in the mRNA transcripts of both
308 PP2A subunits (Fig. 5C). Immunoblotting showed a greater depletion of PP2A protein as
309 compared to knocking down the alpha subunit alone (compare Fig. 5B and D). Upon Δ*yopM*
310 infection PS205 pyrin was maintained and a trend toward decreased IL-1β secretion was
311 observed (Fig. 5D and E). Together, these results implicate PP2A alpha and beta subunits as
312 acting redundantly to dephosphorylate pyrin S205.

313
314
315 DISCUSSION
316
317 In this study, we aimed to understand if a PPP activity is important for positive regulation of
318 inflammasome assembly by oligomeric pyrin. There are seven different PPPs in the mammalian
319 cell: PP1, PP2A, PP2B (PP3), PP4, PP5, PP6 and PP7. In the human genome there are ~428
320 Ser/Thr kinases but only ~30 Ser/Thr phosphatases (50). The remarkable diversity of PPP
321 substrates, substrate recognition and cellular localization is achieved by the association of
322 catalytic subunits with non-catalytic subunits to form multimeric holoenzymes (39). The active
323 sites of these phosphatases share 100% similarity, and most phosphatase inhibitors which bind
324 to the PPP active sites are broadly specific for this reason.
325
326 CA is a relatively non-specific and hydrophobic PPP inhibitor. It can easily partition through cell
327 membranes and potently inhibits most PPPs except for PP2B and PP7 (49). Using 10nM CA we
328 obtained evidence that a PPP activity is important for pyrin S205 dephosphorylation and
329 inflammasome assembly in BMDMs in response to RhoA inactivation by TcdB or YopE/T during
330 Δ*yopM Yptb* infection. The same CA treatment also prevented TecA-dependent
331 dephosphorylation of pyrin S242 in THP-1 cells infected with *B. cenocepacia.* It has been shown
332 previously in mouse peritoneal macrophages that 50nM CA prevented activation of NLRP3, AIM2
333 and NLRC4 inflammasomes, indicating that PPP activity can be important for inflammasome
334 activation in general, and is perhaps acting at a latter step (51). We observed that 10nM CA
335 prevented infection-induced pro-IL-1β synthesis in THP-1 cells infected with *B. cenocepacia*
336 illustrating that results with this inhibitor need to be carefully controlled and interpreted since it
337 can block multiple steps in an inflammasome pathway. Results from our experiments with
338 treatment of BMDMs with CA and Δ*yopK Yptb* mutant infection showed that there was a non-
339 significant decrease in IL-1β release which can be attributed to inhibition of NLRP3 but not of the
340 NLRC4 inflammasome. Luheshi et al used a higher CA concentration of 50nM (51) which could
341 explain why we didn't observe inhibition of NLRC4 inflammasome in response to Δ*yopK* infection
342 with 10nM CA treatment.
343
344 We were also able to show using BN-PAGE that murine pyrin forms oligomers consisting of
345 dimers and higher order oligomers that are phosphorylated on S205 when pyrin is inactive. Due
346 to the insolubility of active pyrin in non-ionic detergent we were unable to determine if

347 dephosphorylation changes the oligomeric status of pyrin. However, PPP inhibition with CA
348 resulted in the appearance of a very high molecular weight mystery oligomer which indicates that
349 phosphorylation increases oligomerization of pyrin. Pyrin belongs to the TRIM family of proteins
350 and Trim5α which is involved in HIV viral capsid recognition is known to form dimers and higher
351 order lattices consisting of dimers of dimers or trimers of dimers (26). The higher order murine
352 pyrin oligomers (~480-720kDa) that we observe on BN-PAGE immunoblots could represent
353 dimers of dimers or trimers of dimers similar to those formed by Trim5α. It has been previously
354 shown through crosslinking studies in THP-1 cell lysates that human pyrin can form trimers which
355 is mediated through its coiled coil domains (28). In the same study it was also shown that the B-
356 box domain of human pyrin interacts with the N-terminal pyrin domain to sequester it and prevent
357 interaction with ASC (28). However, Weinert et al reported that a truncated version of human pyrin
358 forms an antiparallel dimer in vitro through interaction of coiled coil domains (27). These
359 discrepancies in trimer vs dimer formation by human pyrin could be attributed to experimental and
360 technical differences. It is expected that regulation of human and murine pyrin by oligomerization
361 would be conserved but due to structural differences, it is possible that murine pyrin forms dimers
362 and human pyrin forms trimers through their respective coiled coil domains. To rule out technical
363 differences it would be informative to investigate oligomerization of human pyrin by BN-PAGE
364 instead of crosslinking. The phosphorylation status of human pyrin oligomers should also be
365 determined.
366
367 CA treatment resulted in an upshift in molecular weights of PS205 and total murine pyrin bands
368 in all conditions on BN-PAGE immunoblots, as wells as on some SDS-PAGE immunoblots. In
369 addition, CA treatment of THP-1 cells resulted in hyperphosphorylation of S242 in human pyrin.
370 This indicates that a PPP acts constitutively on the second linker site in pyrin to dephosphorylate
371 it and when this PPP is inhibited the second serine becomes hyperphosphorylated. To our
372 knowledge this is the first evidence that one of the linker sites can be hypophosphorylated yet
373 pyrin remains inactive. This finding is surprising given the data that phosphorylation of the second
374 linker site is critical for negative regulation of pyrin, based on alanine substitution of this residue
375 in ectopically expressed pyrin variants (33, 34). In addition, the S242R substitution causes
376 PAAND in which the pyrin variant is considered constitutively active (35). Pull down experiments
377 in this study also showed that 14-3-3 proteins are not bound to the S242R variant and that pyrin
378 is dephosphorylated (35). Jeru et al. showed previously that a S208A pyrin variant has reduced
379 14-3-3 binding while the S242A mutant abolishes 14-3-3 binding (52). This suggested that 14-3-
380 3 binding could follow a gatekeeper hypothesis in which PS242 is the dominant site which

381 promotes 14-3-3 binding and PS208 is a secondary site (52). These findings may indicate that
382 hypophosphorylation of the second linker site is sufficient to keep pyrin oligomers inactive. This
383 could facilitate fast dephosphorylation of the hypophosphorylated second sites, resulting in rapid
384 activation of pyrin in response to RhoA inactivation by pathogens. A caveat of this concept is our
385 limitation of not being able to measure the phosphorylation status of S241 in murine pyrin under
386 the conditions used.
387
388 We were also able to use one and 2D BN-PAGE and immunoblotting to detect interaction of
389 murine pyrin with YopM during WT *Yptb* infection of BMDMs and found that this interaction was
390 sensitive to PPP inhibition. The fact that YopM targets the oligomers argues that they are poised
391 to become activated upon dephosphorylation. We hypothesize that the faint YopM signal on BN-
392 PAGE immunoblots from the *Mefv*$^{-/-}$ BMDMs infected with WT *Yptb* could result from self-
393 oligomerization of the YopM protein. The YopM protein from *Y. pestis* is known to form tetramers
394 in vitro (36, 53), so it is conceivable that the *Yptb* YopM protein can form higher order oligomers
395 on its own in *Mefv*$^{-/-}$ BMDMs. One explanation for the selective loss of the YopM signal at the
396 position of the higher order oligomers from the CA-treated and WT *Yptb*-infected samples is that
397 the affinity of YopM binding to pyrin is reduced by hyperphosphorylation.
398
399 OA in comparison to CA has a greater inhibitory constant to bind to the catalytic subunit of PP2A
400 than of PP1 and is reported to enter cells slowly (54{Swingle, 2007 #2701). Our results indicated
401 that 15min pretreatment with 1000nM OA is sufficient to inhibit S205 pyrin dephosphorylation and
402 IL-1β release in BMDMs upon RhoA inactivation. Stutz et al reported that PP2A is important for
403 NLRP3 activation through dephosphorylation using the same conditions and concentration of OA
404 (42). We only observed a reduction in S205 dephosphorylation and a significant decrease in IL-
405 1β secretion in response to Δ*yopM* infection when BMDMs were pretreated with 100nM OA for
406 3hr but not for 15min, which can be explained by the slow entry of the inhibitor. We hypothesize
407 from these results that PP2A plays a role in dephosphorylation of S205 and positive regulation of
408 the pyrin inflammasome in BMDMs.
409
410 PP2A, along with PP1, carry out most serine/threonine dephosphorylation events in cells and
411 partake in many essential activities for the cell (39). PP2A is abundantly present in cells and forms
412 heterotrimers consisting of a catalytic subunit, a scaffolding A subunit, and a regulatory B subunit
413 (39). There are two isoforms of the catalytic and scaffolding subunits, and four isoforms of the
414 regulatory subunits, which account for the diverse activities and substrates regulated by PP2A

415 (50). The alpha and beta catalytic subunit of PP2A only differ by a few amino acids and PP2Aca
416 is more abundantly present in cells than PP2Acb. Our results indicated that siRNAs targeting
417 PP2Aca did not reduce S205 pyrin dephosphorylation in BMDMs infected with Δ*yopM*. However,
418 a combined knock down of both catalytic subunits of PP2A showed that S205 pyrin
419 phosphorylation was maintained and there was a trend toward decreased in IL-1β secretion upon
420 Δ*yopM* infection. Perhaps the two catalytic subunits of PP2A act redundantly to dephosphorylate
421 the pyrin linker. This is distinct from the case of NLRP3 where knockdown of the alpha catalytic
422 subunit of PP2A alone was sufficient to prevent assembly of the inflammasome (42). To confirm
423 our results, additional siRNAs targeting the alpha and beta catalytic subunit of PP2A should be
424 tested. In addition, the impact of PP2A knockdowns on PS241 in murine pyrin and PS208/242 in
425 human pyrin needs to be investigated.
426
427 PPPs recognize and bind to regulatory proteins or to substrates via short linear motifs (SLiMs)
428 (39). For example, the B56 regulatory subunit of PP2A binds through LxxIxE motifs to its
429 substrates (39). Interestingly, murine pyrin contains two LxxIxE motifs in the coiled-coil domain
430 and human pyrin has one LxxIxE motif in the linker. Since both murine and human pyrin have a
431 PP2A-B56 regulatory motif it is possible that PP2A regulates both forms through a conserved
432 mechanism. This could be tested by inactivation of the SLiM motifs in murine and human pyrin.
433 We have not ruled out the possible roles of other PPPs in pyrin dephosphorylation and
434 inflammasome assembly and additional approaches will likely be needed to address this
435 possibility. Finally, it remains to be determined if the activity of PP2A or other PPP is upregulated
436 upon RhoA inactivation, or these enzymes simply constitutively counterbalance PKN. In the case
437 of PP2A activating NLRP3 by dephosphorylation (42), there is evidence that Bruton tyrosine
438 kinase negatively regulates PP2A by phosphorylation of tyrosine 307 (55). It is theoretically
439 possible that PKN could negatively regulate PPP activities by phosphorylation and additional
440 experiments are needed to address this possibility.
441
442
443 MATERIALS AND METHODS
444
445 **Bacterial strains.** *Y. pseudotuberculosis* (*Yptb*) 32777 (serogroup O1) strains used in this study
446 are as follows: wild-type (56), Δ*yopM* (57), Δ*yopK* (58), *yopE*^{R144A}*ΔyopM* and *yopT*^{C139A}*ΔyopM*
447 (17). *Yptb* was grown at 28°C on Luria broth (LB) agar plates or with shaking in LB broth,
448 supplemented with antibiotics when necessary. The *B. cenocepacia* strains used were AU1054

449 (WT) and Δ*tecA* mutant (59). *B. cenocepacia* was grown at 37°C on LB agar plates or with
450 shaking in LB broth.
451
452 **Bone marrow isolation and cell culture conditions.** Bone marrow derived macrophages
453 (BMDMs) were obtained from femurs of 8-week-old WT C57BL/6 mice (Jackson Laboratories)
454 and/or *Mefv*$^{-/-}$ mice (60) as previously described (19). Cells were grown at 37°C in a humidified
455 incubator in macrophage growth media (MGM) made up of Dulbecco's modified Eagle Medium
456 (DMEM) plus GlutaMAX (Gibco) containing 10% heat inactivated fetal bovine serum (FBS) (GE
457 Health Care), 10% L929 cell-conditioned medium, 1 mM sodium pyruvate (Gibco), 10 mM HEPES
458 (Gibco) for a week. On day 7 differentiated macrophages were divided into six-well plates at a
459 density of 0.8×10^6 cells/well in a total volume of 3 ml in MGM diluted to contain 10% L929 cell-
460 conditioned medium (MGM 10/10) and primed for ~18hrs with 100 ng/ml O26:B6 *Escherichia coli*
461 LPS (Sigma).
462
463 **BMDM infection, intoxication, and inhibitor treatments.** For BMDM infections, *Yptb* strains
464 were grown overnight in LB at 28°C. The following day, cultures were diluted 1:40 in LB containing
465 20 mM sodium oxalate and 20 mM MgCl2 and grown at 28°C for 1 hr, then shifted to 37°C for 2
466 hr. Cultures were centrifuged and the bacterial pellets were resuspended in phosphate-buffered
467 saline (PBS). Bacterial suspensions were then diluted in media lacking FBS and containing 10%
468 L929 cell-conditioned medium (MGM 0/10). LPS-primed BMDMs were washed once with PBS
469 and left uninfected or infected in MGM 0/10 with *Yptb* strains cultured under conditions as
470 described above at an MOI of 30. Plates were centrifuged for 5 min at 106xg to facilitate contact
471 between *Yptb* and macrophages. Plates were then incubated at 37°C in 5% CO_2. In experiments
472 where the glucosyltransferase toxin TcdB from *Clostridium difficile* (List Biological Laboratories,
473 Inc.) was used as a positive control for pyrin inflammasome activation, BMDMs were intoxicated
474 with TcdB at a concentration of 0.1 μg/ml for 90min in MGM 0/10 media.
475
476 In experiments where phosphatase inhibitors were used and BMDMs were pre-treated for 15min
477 with either 1.4mM DMSO as vehicle control or calyculin A (10nM diluted from 100μM stock, LC
478 Laboratories), cyclosporin A (1μM diluted from 1mM stock, Sigma), okadaic acid (100nM or 1μM
479 diluted from 1mM stock, Tocris), or tautomycetin (1μM or 2μM diluted from 1mM stock, Tocris) in
480 MGM 0/10. MGM 10/10 was used for BMDMs pre-treated for 3hr with 100nM okadaic acid. For
481 infection following pre-treatment, MGM 0/10 media containing bacteria and DMSO or the
482 respective phosphatase inhibitors was added to the BMDMs, followed by centrifugation and

483 incubation as above. Post-infection, cell supernatants were collected and processed for IL-1β
484 detection by ELISA and cell lysates were prepared and processed for immunoblot analysis (see
485 below).
486
487 **THP-1 cells, infection, and inhibitor treatment.** THP-1 cells (ATCC TIB-202) were grown in
488 filter sterilized RPMI 1640 media (Cat. No 30-2001) containing 10% heat inactivated fetal bovine
489 serum and 1.7μl 14.3M β-mercaptoethanol (to prevent cells from clumping) in 25cm^2 flasks.
490 When confluent the THP-1 cells were expanded in 75cm^2 flasks. No cells were used that were
491 passaged more than 30 times. For infections, THP-1 cells were seeded at a density of 0.8x10^6
492 cells per well in 1.5ml of media in 6-well plates and pretreated with ? mM DMSO vehicle control
493 or 10nM calyculin A for 15 min. Overnight (16-hour) cultures of *B. cenocepacia* were subcultured
494 1:100 in fresh LB on infection day and shaken at 37°C until the cultures reached mid-log phase
495 (OD_{600} = 0.300). Cultures were then centrifuged, the LB was removed, and the bacterial pellets
496 were resuspended in PBS and then diluted to an MOI of 20 in warmed RPMI 1640 media without
497 FBS and containing DMSO or calyculin A. 1.5ml of supplemented media was added to each well
498 and mixed by pipetting gently up and down. Following incubation for 3 hours at 37°C, the contents
499 of each well was collected and centrifuged for 10 minutes at 14,000rpm and 4°C. The cell pellet
500 was collected and lysed for immunoblot analysis as described below.
501
502 **Protein analysis by SDS-PAGE and immunoblotting.** To obtain cell lysates, BMDMs and THP-
503 1 cells were lysed in mammalian protein extraction reagent (MPER, Thermo Scientific) along with
504 cOmplete Mini (Roche) protease inhibitor and PhosSTOP (Roche) phosphatase inhibitor. The
505 lysis buffer for THP-1 cells was supplemented with 10 nM calyculin A. Protein concentration was
506 normalized after measurement with a bichinonic acid assay (BCA, Thermo Fisher Scientific) and
507 3-10μg of total protein cell lysates was run on 4 to 12% NuPAGE Bis-Tris SDS-PAGE gels
508 (Invitrogen by ThermoFisher Scientific) and transferred to polyvinylidene difluoride membranes
509 (ThermoFisher Scientific) using an iBlot 2 gel transfer device (Life Technologies). Membranes
510 were blocked in 5% nonfat dairy milk (add company) and incubated with primary antibodies
511 overnight. Primary antibodies used in this paper were: rabbit-anti-mouse monoclonal total pyrin
512 antibody (1:1000 dilution, ab195975; abcam), rabbit-anti-mouse pyrin polyclonal (1:1000 dilution,
513 (60)), rabbit-anti-mouse phospho-serine 205 monoclonal antibody (1:1000 dilution, ab201784;
514 abcam), rabbit-anti-mouse phospho-serine 241 monoclonal antibody (1:1000 dilution, ab201784;
515 abcam), rabbit-anti-mouse/human IL-1β (1:1000 dilution, number 12242; Cell Signaling), rabbit-
516 anti-mouse/human polyclonal β-actin (1:1000 dilution, number 4967; Cell Signaling), mouse-anti-

517 mouse/human/rat monoclonal PP1a (1:1000 dilution, number MA5-17239, ThermoFisher
518 Scientific), rabbit-anti-*Y.pestis* polyclonal YopM (1:1000 dilution, provided by Susan Straley),
519 mouse-anti-mouse monoclonal PKN (1:1000 dilution, number 393344, Santa Cruz
520 Biotechnology), rabbit-anti-mouse monoclonal PP2A (1:1000 dilution, #2038, Cell Signaling), and
521 rabbit-anti-mouse GSDMD (1:1000 dilution, ab209845, Abcam). Horseradish peroxidase-
522 conjugated anti-rabbit or mouse antibody (Jackson Laboratory) were used as secondary
523 antibodies. Protein bands bound by antibodies were visualized using chemiluminescent detection
524 reagent (GE Healthcare) on an iBright FL1500 (ThermoFisher Scientific).
525
526 **Protein analysis by blue native (BN)-PAGE and immunoblotting.** BN-PAGE immunoblotting
527 was performed as described by Kofoed and Vance (45). All reagents for this procedure were
528 obtained from Invitrogen except as stated. BMDMs were lysed in non-denaturing 1X Native-PAGE
529 Novex sample buffer with the indicated concentrations of either digitonin (5% stock) or DDM (10%
530 stock), MPER (Thermo Scientific) or RIPA lysis or extraction buffer (Thermo Scientific), along with
531 cOmplete Mini (Roche) protease inhibitor and PhosSTOP (Roche) phosphatase inhibitor. Lysates
532 were centrifuged at 20,817xg for 10min to obtain soluble and insoluble fractions. In some
533 experiments the insoluble fractions of 1% digitonin lysates were analyzed by SDS-PASGE and
534 immunoblotting as described above. Protein concentrations of soluble fractions were normalized
535 after measurement with a bichinonic acid assay (BCA, Thermo Fisher Scientific) and 10µg or
536 more of total protein cell lysates was mixed with NativePAGE G-250 additive and loaded on 4-
537 16% NativePAGE Novex 3–12 % Bis-Tris gels. NativeMark unstained protein standard was used
538 for molecular weight standard visualization. XCell SureLock Mini-Cell was used for running the
539 gels. Samples were run at room temperature (RT) at constant 150V for 105-120min using pre-
540 chilled buffers. Dark blue cathode buffer (10ml NativePAGE running buffer, 10ml NativePAGE
541 cathode additive, 180ml deinonized water) was used for the inner chamber 17ntil samples had
542 run up to 1/3rd of the gel length after which the buffer was replaced with light blue buffer (10ml
543 NativePAGE running buffer, 1ml NativePAGE cathode additive, 189ml deinonized water) for the
544 remainder of the run. The outer chamber was filled with NativePAGE running buffer. Gels were
545 soaked in 2X NuPAGE transfer buffer (Invitrogen) for 15min at shaking at room temperature.
546 Proteins were transferred to polyvinylidene difluoride membranes (ThermoFisher Scientific) using
547 the template program P3 (20V constant, 7min) and an iBlot 2 gel transfer device (Life
548 Technologies). Post transfer membranes were incubated in 8% acetic acid for 15min with shaking,
549 followed by ponceau S staining for 5min. Membranes were washed with distilled water for 5min

550 to remove excess ponceau S stain then air-dried, reactivated by immersion in methanol, followed
551 by blocking in 5% non-fat dry milk. Primary and secondary antibodies used are mentioned above.
552
553 **Protein analysis by two-dimensional blue native (BN)-PAGE and immunoblotting.** The
554 procedures used followed a previously described protocol (45). Samples were prepared as
555 described above and separated on NativePAGE Novex 3–12 % Bis-Tris gels. Gel slices
556 containing samples of interest were excised, trimmed to be 3mm shorter in length than the size
557 of the 2D well in NuPAGE 4–12 % Bis-Tris 2D Gels, then submerged and shaken at RT in 1X
558 NuPAGE sample buffer containing 0.1M DTT. Gel slices wwere then microwaved for ~20sec to
559 denature proteins followed by cooling with shaking at 10min at RT. Slices were then fitted into the
560 2D well and SDS-PAGE immunoblotting was performed as described above.
561
562 **siRNA knock-down.** siRNAs targeting *Pkn1* (s115927), *PP2Aca* (#1: s72067, #2: s72066) and
563 *PP2Acb* (#1: s72069) were obtained from Invitrogen. For siRNA gene knock-down experiments,
564 400pmol of *Pkn1*,1000pmol of *PP2Aca* siRNAs, and for combined PP2Ac knock down, 500pmol
565 each of PP2Aca #2 siRNA and PP2Acb #1 siRNA were transfected into BMDMs (1×10^6 cells) by
566 electroporation using the Neon Transfection System (Invitrogen) and electrical parameters of
567 1400V, 20ms and 2 pulses. BMDMs were then replated in 6-well plates and grown in MGM 10/10
568 media. 24hr following transfection, media was changed to fresh MGM 10/10 and LPS was added
569 for overnight incubation. 48hr following transfection BMDMs were infected with Δ*yopM Yptb* as
570 described above.
571
572 **Quantitative real-time PCR (RT-qPCR).** At 48hr following transfection, uninfected BMDMs were
573 lysed with trizol reagent (Invitrogen) to isolate RNA according to the manufacturer's instructions.
574 500-1000ng of RNA was used to make cDNA using SuperScript IV First-Strand Synthesis System
575 (Invitrogen). Approximately ~5ng of cDNA was quantified using PowerUp SYBR Green Master
576 Mix (Invitrogen) in the (add machine name). Primer specificity was checked by melt-curve
577 analysis. Expression of target genes was normalized to the expression of the housekeeping gene
578 Hprt. For fold change analysis data was transformed using the 'relative standard curve method
579 and comparative threshold cycle (Ct) method (ΔΔCt)' as described by Applied Biosystems.
580 Published primer sequences were used for qPCR analysis (42) and the sequences are: Hprt,
581 forward 5′-TGAAGT ACTCATTATAGTCAAGGGCA-3′ and reverse 5′-CTG
582 GTGAAAAGGACCTCTCG-3′; Ppp2ca, forward 5′-TCTTCCTCTCACTGCCTTGGT-3′ and

583 reverse 5′-CAG CAAGTCACACATTGGACCC-3′; Ppp2cb, forward 5′-
584 AAGGCGTTCACCAAGGAGCT-3′ and reverse 5′- ACAGCGGACCTCTTGCACAT-3′.
585
586 **IL-1β quantification.** IL-1β in BMDM supernatants was quantified using a murine ELISA kit
587 (MLB00C; R&D Systems) by following the manufacturer's instructions.
588
589 **Statistical analysis.** GraphPad Prism was used to perform statistical analyses. IL-1β ELISA data
590 were analyzed by one-way or two-way analysis of variance (ANOVA; Tukey's multiple-
591 comparison test).
592
593 **Acknowledgments.** We thank Isha Nasa for help in providing advice on the phosphatase
594 inhibitors used in Fig. S1. We would also like to thank members of the Bliska lab for providing
595 helpful suggestions towards this project.
596

FIGURES

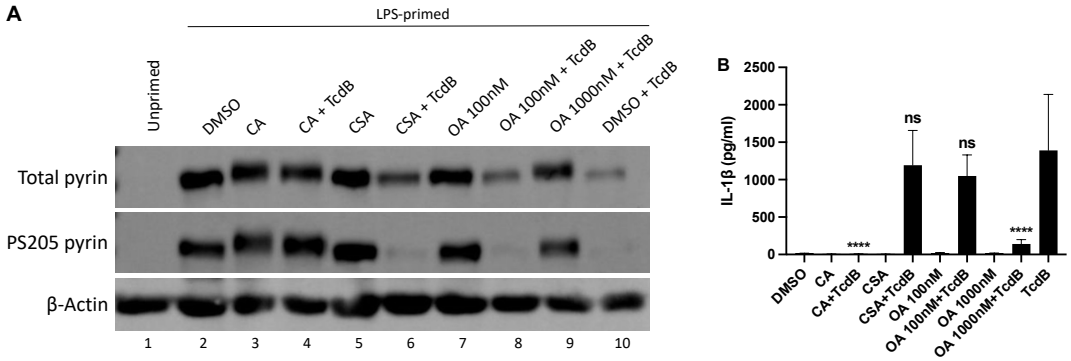

Fig.S1. PPP inhibition with CA and OA prevents pyrin S205 dephosphorylation and reduces IL-1β release in BMDMs intoxicated with TcdB. LPS-primed BMDMs were pretreated for 15mins and maintained with either 10nM calyculin A (CA), 100nM okadaic acid (OA), 1000nM OA or 1000nM cyclosporin A (CSA), and left unintoxicated or intoxicated with 0.1μg/mL of TcdB for 90 mins. Unprimed BMDMs or treatment with vehicle DMSO were used as controls. A) Immunoblot analysis of total and PS205 pyrin in BMDM lysates. Actin was used as a loading control. B) Mature IL-1β in supernatants as quantified by ELISA. Two-way ANOVA with Bonferroni post hoc correction was applied to calculate significance and p-values as compared to DMSO+TcdB are indicated. P-value<0.05 was considered significant; <0.0001 (****); not significant (ns). Each data group is presented as an average (error bars are standard deviation) of at least 3 independent experiments.

611

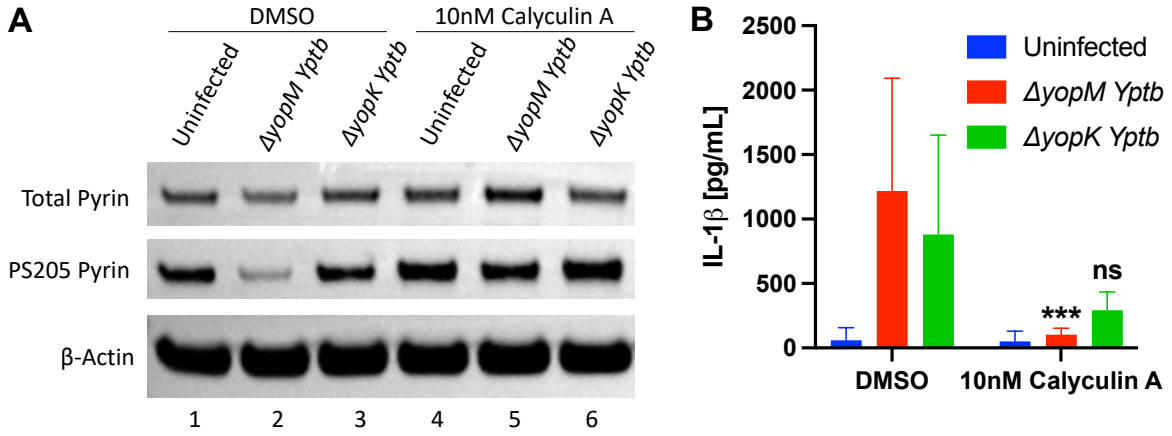

612
613 Fig.1. PPP inhibition with CA reduces pyrin dephosphorylation and IL-1β release in BMDMs
614 infected with Δ*yopM Yptb.* LPS-primed BMDMs were pre-treated for 15mins and maintained with
615 either DMSO or 10nM CA, and infected with the Δ*yopM* or Δ*yopK* strain at an MOI of 30 for 90
616 mins. Treated uninfected BMDMs were analyzed in parallel. A) Immunoblot analysis of PS205
617 and total pyrin in BMDM lysates. Actin was used as a loading control. B) Mature IL-1β in
618 supernatants as quantified by ELISA. Two-way ANOVA with Bonferroni post hoc correction was
619 applied to calculate significance and p-values of each treatment as compared to its corresponding
620 DMSO treated infected strain is indicated. P-value<0.05 was considered significant; <0.001 (***);
621 not significant (ns). Each data group is presented as an average (error bars are standard
622 deviation) of at least 3 independent experiments.
623

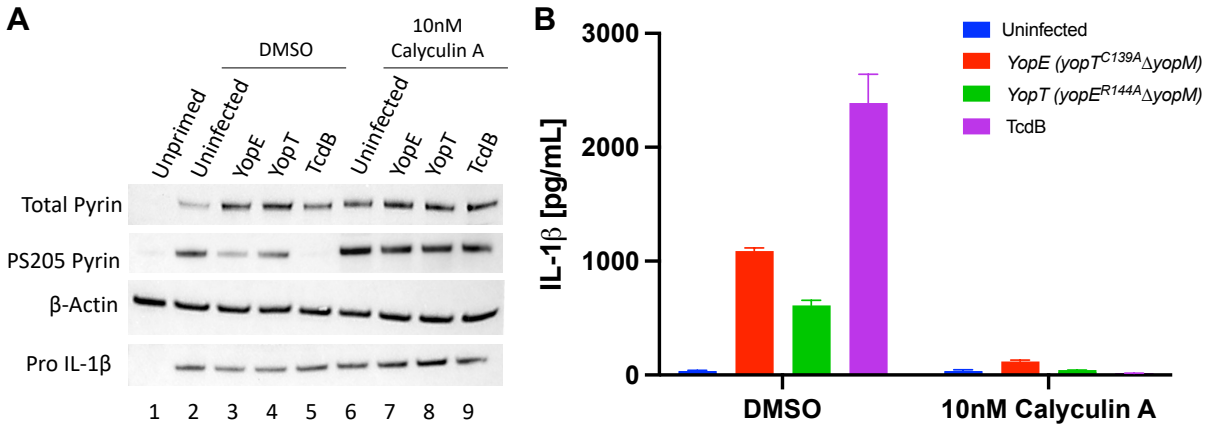

Fig.S2. PPP inhibition with CA reduces pyrin dephosphorylation and IL-1β release in BMDMs infected with Δ*yopM Yptb* strains expressing only active YopE or YopT. LPS-primed BMDMs were pre-treated for 15min and maintained with either DMSO or 10nM CA, and either infected with the Δ*yopM Yptb* YopE (*yopT*^{C139A}) or YopT (*yopE*^{R144A}) strains at an MOI of 30 or intoxicated with 0.1µg/mL of TcdB for 90 mins. Unprimed and uninfected BMDMs were analyzed in parallel as controls. A) Immunoblot analysis of PS205 and total pyrin and pro-IL-1β in BMDM lysates. Actin was used as a loading control. B) Mature IL-1β in supernatants as quantified by ELISA. Each data group is presented as an average (error bars are standard deviation) of two technical replicates.

637
638

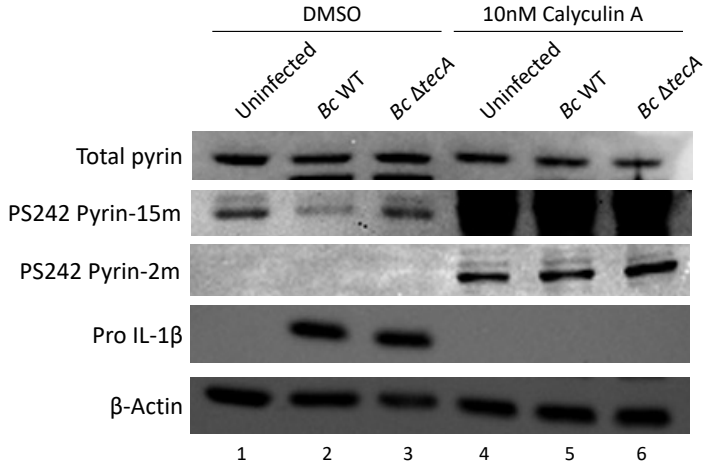

639
640 Fig.S3. PPP inhibition with CA results in hyperphosphorylation of pyrin S242. Naïve THP-1 cells
641 were pre-treated for 15 min and maintained with either DMSO or 10nM CA, and either left
642 uninfected or infected with *B. cenocepacia* (Bc) WT or Δ*tecA* for 180 min at an MOI of 20.
643 Immunoblot analysis of total and PS242 pyrin and pro-IL-1β in THP-1 lysates is shown. PS242
644 pyrin signals are show with long (15m) or short (2m) exposures for comparison. Actin was
645 immunoblotted as a loading control.
646

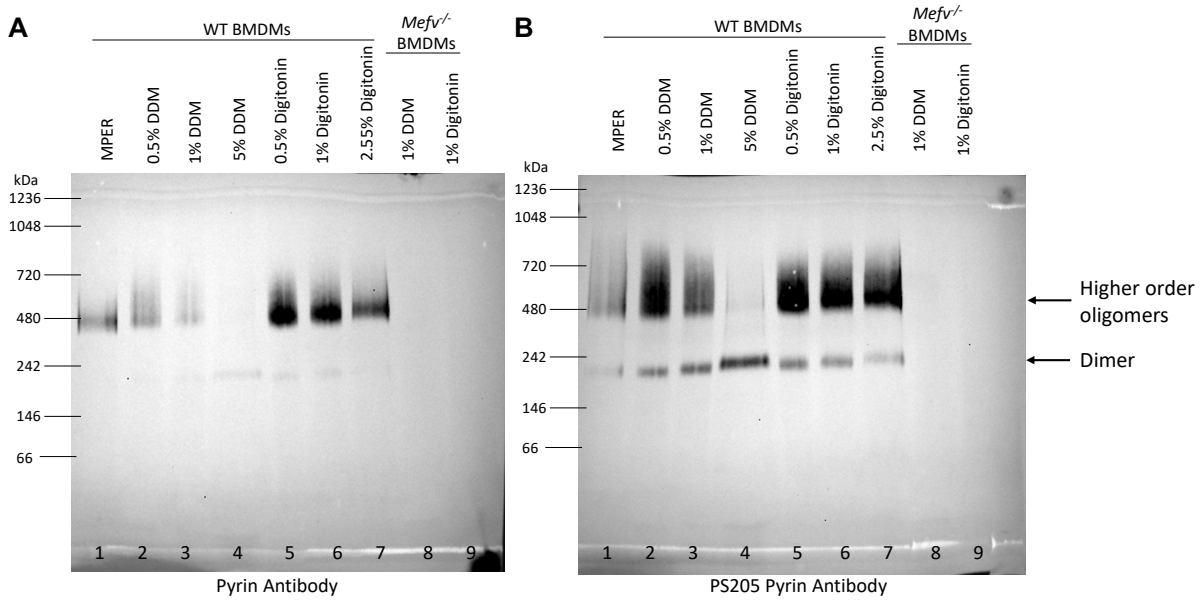

Fig.S4. BMDM lysates prepared with digitonin are optimal for detection of pyrin oligomers using BN-PAGE and immunoblotting. LPS-primed WT and *Mefv*$^{-/-}$ BMDMs were lysed in various non-ionic detergent concentrations as indicated. Lysate samples were separated by BN-PAGE and immunoblotted to visualize total (A) and PS205 pyrin (B) oligomers. Positions of BN-PAGE molecular weight standards are shown on the left of each panel, and dimer and higher order oligomer are indicated on the right of (B).

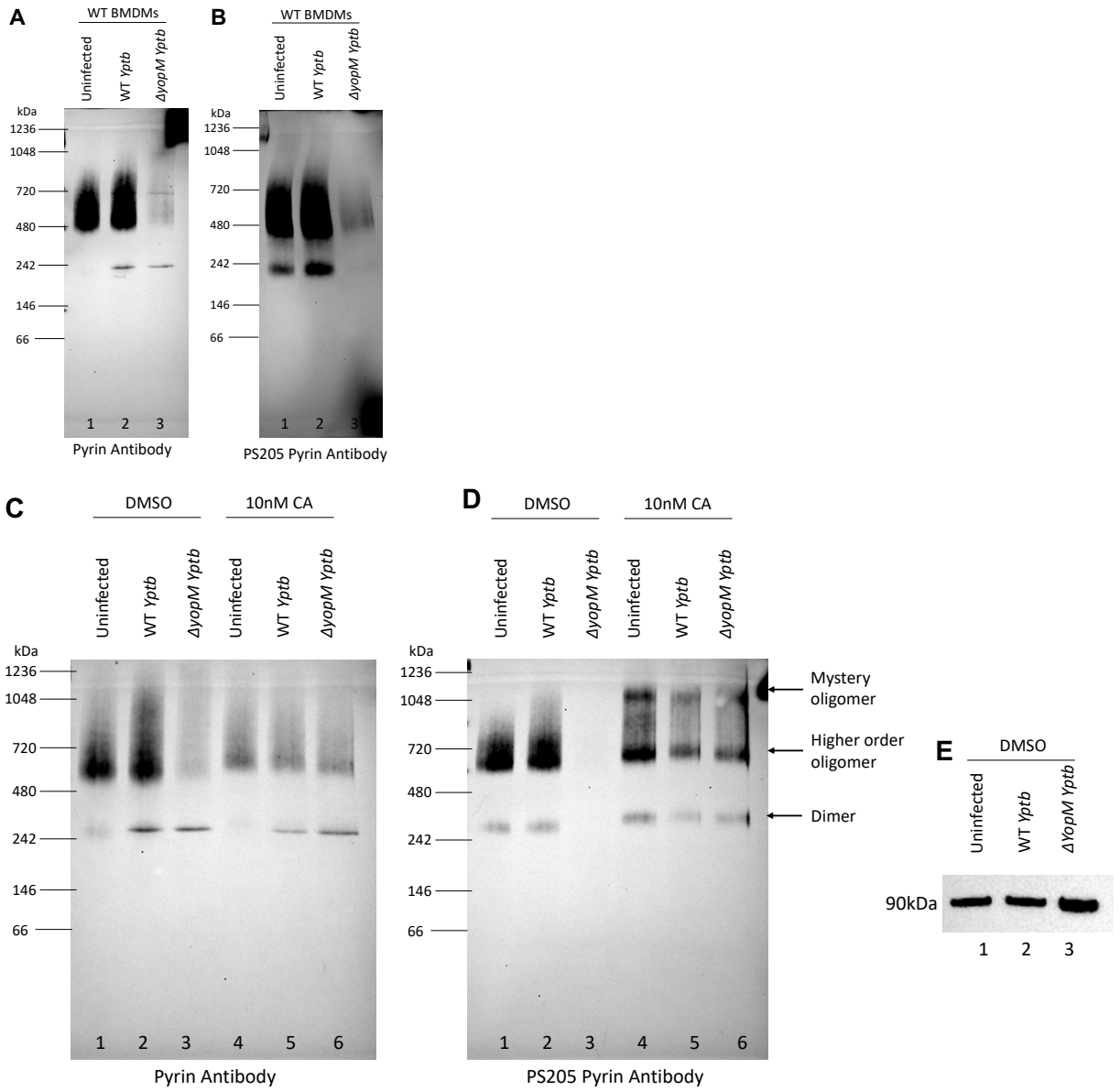

Fig.2. Impact of PPP inhibition with CA and *Yptb* infection on pyrin oligomers and phosphorylation as determined by BN-PAGE and immunoblotting. WT BMDMs left untreated (A,B) or pre-treated and maintained with DMSO or 10 nM CA (C-E) were left uninfected or infected with WT or Δ*yopM Yptb* at an MOI of 30 for 90 mins. BMDM lysate samples prepared in 1% digitonin were separated by BN-PAGE and immunoblotted for total (A,C) or PS205 (B,D) pyrin. BN-PAGE MW standards are shown on the left and tentative positions of pyrin oligomers are shown on the right. Insoluble proteins from 1% digitonin lysates of DMSO treated samples were analyzed by SDS-PAGE and total pyrin immunoblotting (E).

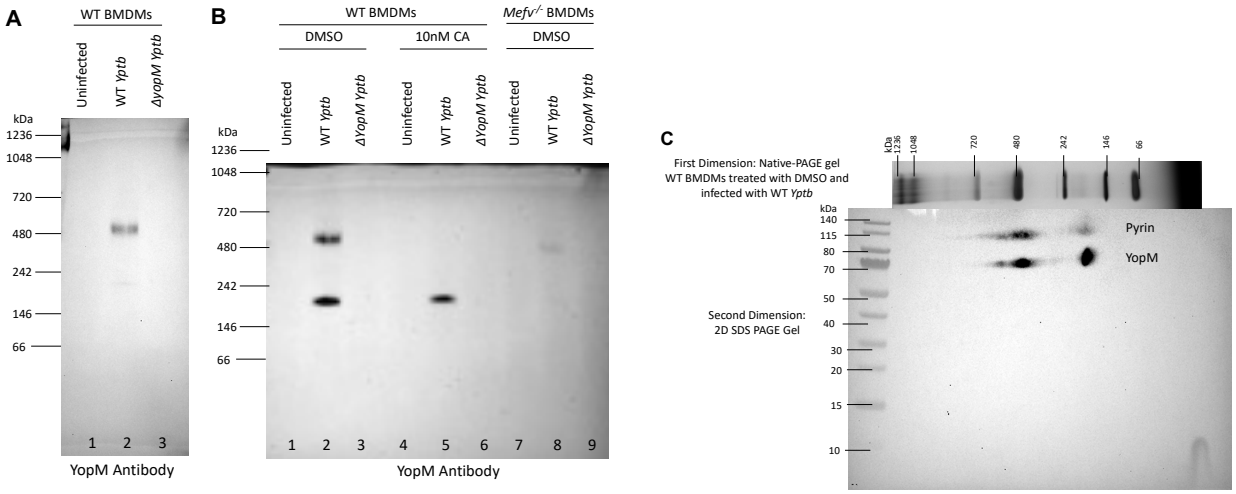

Fig.3. Detection of YopM interaction with pyrin oligomers by one-dimensional and two-dimensional BN-PAGE and immunoblotting. Untreated WT BMDMs (A) or WT or *Mefv*$^{-/-}$ BMDMs pre-treated for 15 min and maintained in DMSO or CA (B, C) were either left uninfected or infected with WT or Δ*yopM Yptb* at an MOI of 30 for 90 mins. Cell lysates were solubilized in 1% digitonin, separated by one dimensional BN-PAGE and immunoblotted for YopM (A,B). BN-PAGE MW standards are shown on the left and tentative positions of YopM oligomers are shown on the right. C) A 1% digitonin sample from WT BMDMS treated with DMSO and infected with WT *Yptb* was separated in the first dimension by BN-PAGE after which the gel slice was isolated and analyzed by SDS-PAGE in the second dimension followed by immunoblotting for pyrin and YopM. MW markers for each dimension are indicated.

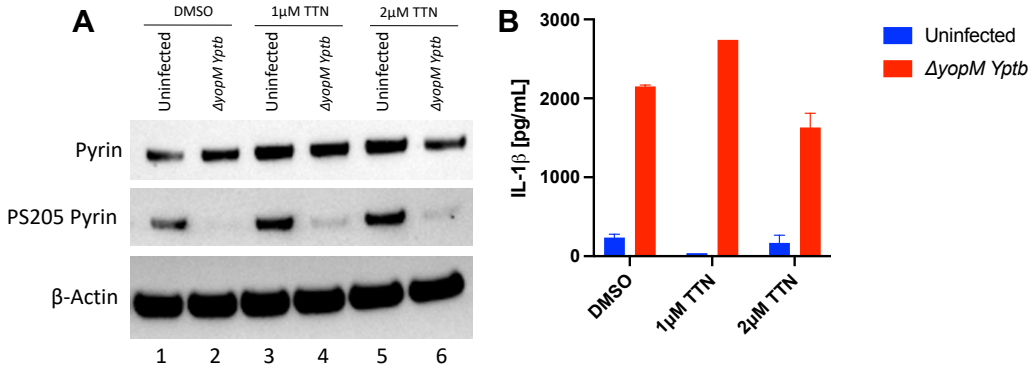

Fig.S4. TTN treatment does not reduce dephosphorylation of pyrin or IL-1β release in BMDMs infected with Δ*yopM Yptb.* LPS-primed BMDMs were pre-treated for 15 mins and maintained with either DMSO or 1 or 2μM TTN and infected with Δ*yopM Yptb* at an MOI of 30 for 90 mins. Treated uninfected BMDMs were analyzed in parallel. A) Immunoblot analysis of PS205 and total pyrin in BMDM lysates. Actin was used as a loading control. B) Mature IL-1β in supernatants as quantified by ELISA. Each data group is presented as an average (error bars are standard deviation) of technical replicates from one experiment.

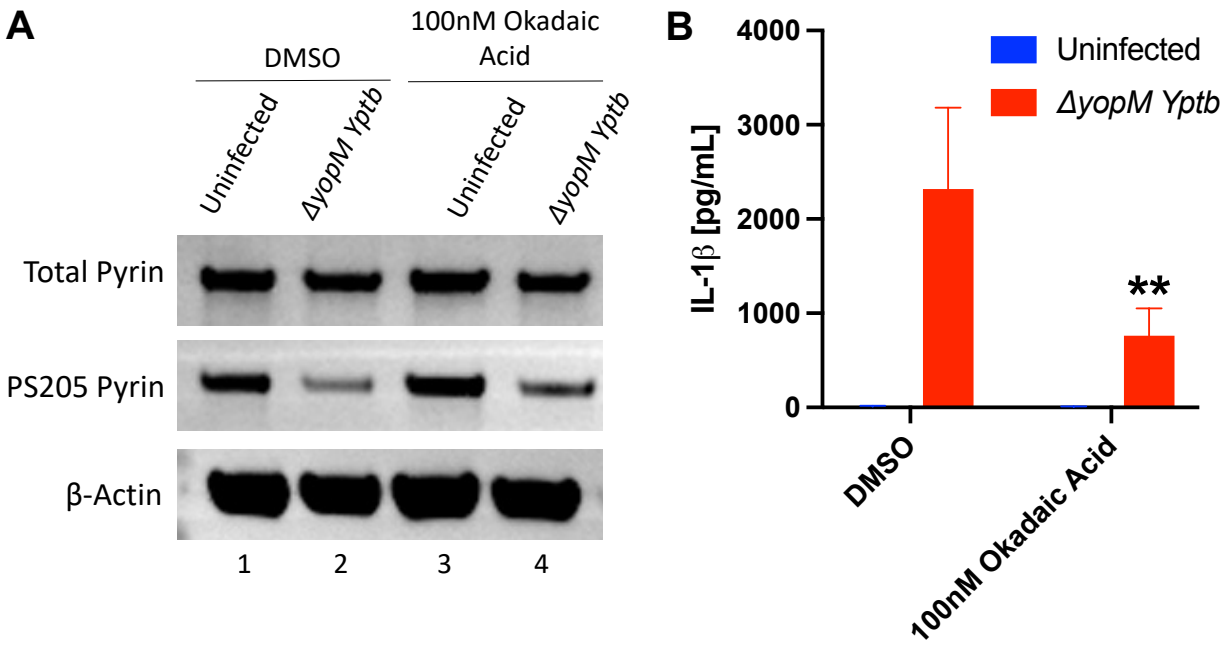

Fig. 4. Longer pretreatment with 100nM OA reduces pyrin dephosphorylation and IL-1β release in BMDMs infected with Δ*yopM Yptb.* LPS-primed BMDMs were pre-treated for 3 hrs and maintained with either DMSO or 100nM OA and infected with the Δ*yopM Yptb* at an MOI of 30 for 90 mins. Treated uninfected BMDMs were analyzed in parallel. A) Immunoblot analysis of PS205 and total pyrin in BMDM lysates. Actin was used as a loading control. B) Mature IL-1β in supernatants as quantified by ELISA. Two-way ANOVA with Bonferroni post hoc correction was applied to calculate significance and p-value of OA treatment as compared to its corresponding DMSO treated and Δ*yopM* infected sample is indicated. P-value<0.05 was considered significant; <0.01 (**). Each data group is presented as an average (error bars are standard deviation) of at least 3 independent experiments.

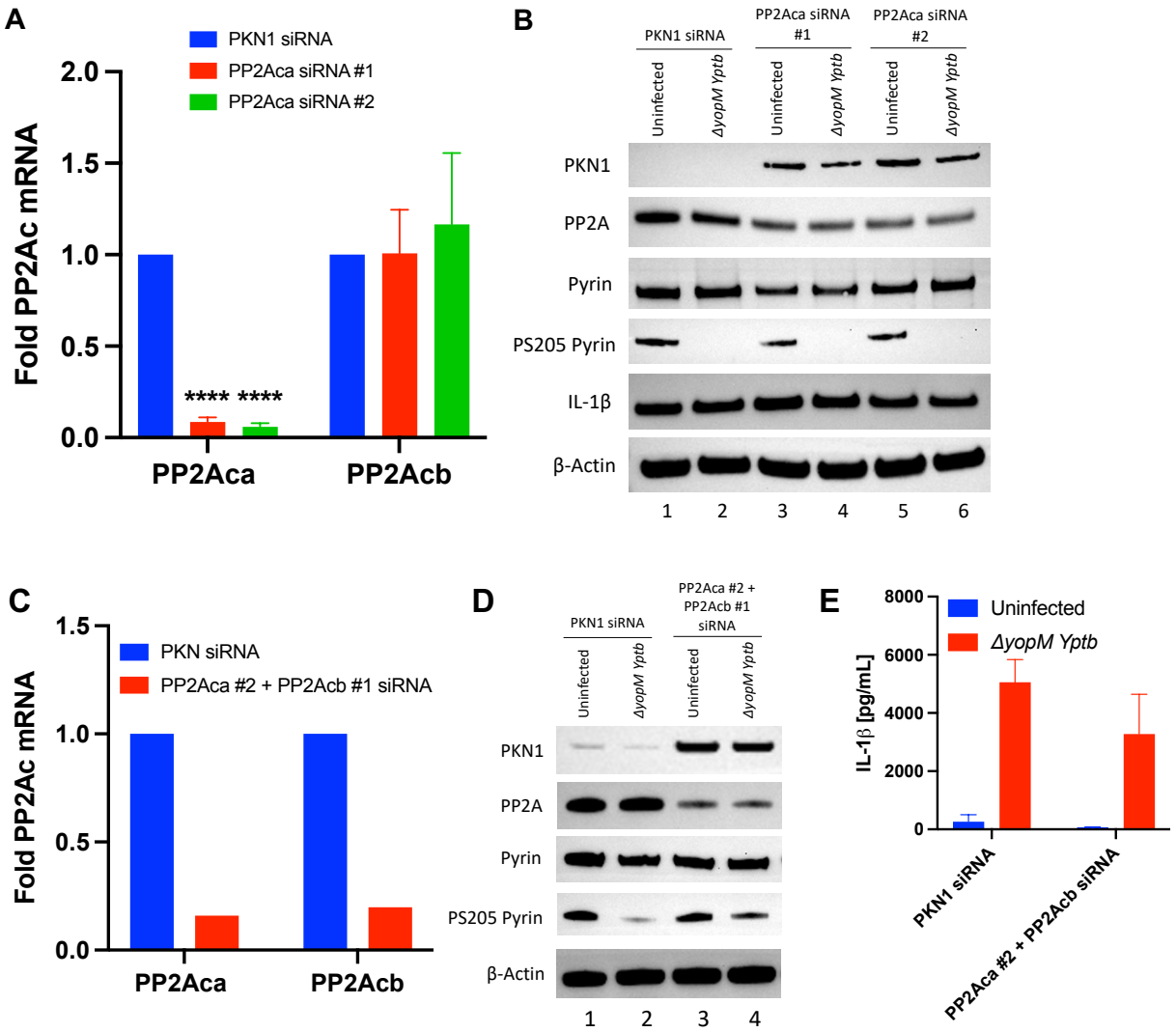

Fig. 5. siRNA knock down of PP2A in BMDMs reduces pyrin S205 dephosphorylation. WT BMDMs were electroporated with siRNAs targeting PKN1 (400pmol), PP2Aca (1000pmol) or PP2Aca+PP2Acb (500pmol each) as indicated. 24hr after electroporation the BMDMs were LPS-primed. 48hr following electroporation, cells were either left uninfected or infected with Δ*yopM Yptb* at an MOI of 30 for 90 mins. A and C) RT-qPCR analysis of mRNA transcripts of PP2Aca and PP2Acb in uninfected BMDMs. Results were normalized to Hprt mRNA levels. A) Each data group is presented as an average (error bars are standard deviation) of three independent experiments. One-way ANOVA was applied to calculate significance and p-values as compared to PKN1 control siRNA are indicated. P-value<0.05 was considered significant; <0.0001 (****). C) Results from one experiment are shown. B, and D) Immunoblot analysis of PKN1, PP2A, total and PS205 pyrin, and pro-IL-1β in uninfected and Δ*yopM Yptb*-infected BMDM lysates. Actin was used as a loading control. E) Mature IL-1β in supernatants as quantified by ELISA. Results represent averages (error bars are standard deviation) from two independent experiments.

REFERENCES

1. Troisfontaines P, Cornelis GR. 2005. Type III secretion: more systems than you think. Physiology (Bethesda) 20:326-39.
2. Raymond B, Young JC, Pallett M, Endres RG, Clements A, Frankel G. 2013. Subversion of trafficking, apoptosis, and innate immunity by type III secretion system effectors. Trends Microbiol 21:430-41.
3. Blander JM, Sander LE. 2012. Beyond pattern recognition: five immune checkpoints for scaling the microbial threat. Nat Rev Immunol 12:215-25.
4. Vance RE, Isberg RR, Portnoy DA. 2009. Patterns of pathogenesis: discrimination of pathogenic and nonpathogenic microbes by the innate immune system. Cell Host Microbe 6:10-21.
5. Sollberger G, Strittmatter GE, Garstkiewicz M, Sand J, Beer HD. 2014. Caspase-1: the inflammasome and beyond. Innate Immun 20:115-25.
6. Shin S, Brodsky IE. 2015. The inflammasome: Learning from bacterial evasion strategies. Semin Immunol doi:10.1016/j.smim.2015.03.006.
7. Kovacs SB, Miao EA. 2017. Gasdermins: Effectors of Pyroptosis. Trends Cell Biol doi:10.1016/j.tcb.2017.05.005.
8. Shi J, Gao W, Shao F. 2017. Pyroptosis: Gasdermin-Mediated Programmed Necrotic Cell Death. Trends Biochem Sci 42:245-254.
9. Shi J, Zhao Y, Wang K, Shi X, Wang Y, Huang H, Zhuang Y, Cai T, Wang F, Shao F. 2015. Cleavage of GSDMD by inflammatory caspases determines pyroptotic cell death. Nature 526:660-5.
10. Bergsbaken T, Fink SL, den Hartigh AB, Loomis WP, Cookson BT. 2011. Coordinated host responses during pyroptosis: caspase-1-dependent lysosome exocytosis and inflammatory cytokine maturation. J Immunol 187:2748-54.
11. Brewer SM, Brubaker SW, Monack DM. 2019. Host inflammasome defense mechanisms and bacterial pathogen evasion strategies. Curr Opin Immunol 60:63-70.
12. Cornelis GR. 2006. The type III secretion injectisome. Nat Rev Microbiol 4:811-25.
13. Viboud GI, Bliska JB. 2005. Yersinia outer proteins: role in modulation of host cell signaling responses and pathogenesis. Annu Rev Microbiol 59:69-89.
14. Black DS, Bliska JB. 2000. The RhoGAP activity of the *Yersinia pseudotuberculosis* cytotoxin YopE is required for antiphagocytic function and virulence. Mol Microbiol 37:515-527.

753 15. Shao F, Vacratsis PO, Bao Z, Bowers KE, Fierke CA, Dixon JE. 2003. Biochemical
754 characterization of the *Yersinia* YopT protease: cleavage site and recognition elements
755 in Rho GTPases. Proc Natl Acad Sci USA 100:904-909.
756 16. LaRock CN, Cookson BT. 2012. The Yersinia virulence effector YopM binds caspase-1
757 to arrest inflammasome assembly and processing. Cell Host Microbe 12:799-805.
758 17. Chung LK, Park YH, Zheng Y, Brodsky IE, Hearing P, Kastner DL, Chae JJ, Bliska JB.
759 2016. The Yersinia Virulence Factor YopM Hijacks Host Kinases to Inhibit Type III
760 Effector-Triggered Activation of the Pyrin Inflammasome. Cell Host Microbe 20:296-306.
761 18. Ratner D, Orning MP, Proulx MK, Wang D, Gavrilin MA, Wewers MD, Alnemri ES,
762 Johnson PF, Lee B, Mecsas J, Kayagaki N, Goguen JD, Lien E. 2016. The Yersinia
763 pestis Effector YopM Inhibits Pyrin Inflammasome Activation. PLoS Pathog
764 12:e1006035.
765 19. Brodsky IE, Palm NW, Sadanand S, Ryndak MB, Sutterwala FS, Flavell RA, Bliska JB,
766 Medzhitov R. 2010. A Yersinia Effector Protein Promotes Virulence by Preventing
767 Inflammasome Recognition of the Type III Secretion System. Cell Host Microbe 7:376-
768 387.
769 20. Zwack EE, Snyder AG, Wynosky-Dolfi MA, Ruthel G, Philip NH, Marketon MM, Francis
770 MS, Bliska JB, Brodsky IE. 2015. Inflammasome activation in response to the Yersinia
771 type III secretion system requires hyperinjection of translocon proteins YopB and YopD.
772 MBio 6:e02095-14.
773 21. Malik HS, Bliska JB. 2020. The pyrin inflammasome and the Yersinia effector interaction.
774 Immunol Rev 297:96-107.
775 22. Medici NP, Rashid M, Bliska JB. 2019. Characterization of pyrin dephosphorylation and
776 inflammasome activation in macrophages as triggered by the Yersinia effectors YopE
777 and YopT. Infect Immun doi:10.1128/IAI.00822-18.
778 23. Xu H, Yang J, Gao W, Li L, Li P, Zhang L, Gong YN, Peng X, Xi JJ, Chen S, Wang F,
779 Shao F. 2014. Innate immune sensing of bacterial modifications of Rho GTPases by the
780 Pyrin inflammasome. Nature 513:237-41.
781 24. Aubert DF, Xu H, Yang J, Shi X, Gao W, Li L, Bisaro F, Chen S, Valvano MA, Shao F.
782 2016. A Burkholderia Type VI Effector Deamidates Rho GTPases to Activate the Pyrin
783 Inflammasome and Trigger Inflammation. Cell Host Microbe 19:664-74.
784 25. Schnappauf O, Chae JJ, Kastner DL, Aksentijevich I. 2019. The Pyrin Inflammasome in
785 Health and Disease. Front Immunol 10:1745.

786 26. Ganser-Pornillos BK, Pornillos O. 2019. Restriction of HIV-1 and other retroviruses by
787 TRIM5. Nat Rev Microbiol 17:546-556.
788 27. Weinert C, Morger D, Djekic A, Grutter MG, Mittl PR. 2015. Crystal structure of TRIM20
789 C-terminal coiled-coil/B30.2 fragment: implications for the recognition of higher order
790 oligomers. Sci Rep 5:10819.
791 28. Yu JW, Fernandes-Alnemri T, Datta P, Wu J, Juliana C, Solorzano L, McCormick M,
792 Zhang Z, Alnemri ES. 2007. Pyrin activates the ASC pyroptosome in response to
793 engagement by autoinflammatory PSTPIP1 mutants. Mol Cell 28:214-27.
794 29. Chae JJ, Centola M, Aksentijevich I, Dutra A, Tran M, Wood G, Nagaraju K, Kingma
795 DW, Liu PP, Kastner DL. 2000. Isolation, genomic organization, and expression analysis
796 of the mouse and rat homologs of MEFV, the gene for familial mediterranean fever.
797 Mamm Genome 11:428-35.
798 30. Gao W, Yang J, Liu W, Wang Y, Shao F. 2016. Site-specific phosphorylation and
799 microtubule dynamics control Pyrin inflammasome activation. Proc Natl Acad Sci U S A
800 113:E4857-66.
801 31. Jones JD, Dangl JL. 2006. The plant immune system. nature 444:323-329.
802 32. Thumkeo D, Watanabe S, Narumiya S. 2013. Physiological roles of Rho and Rho
803 effectors in mammals. Eur J Cell Biol 92:303-15.
804 33. Park YH, Wood G, Kastner DL, Chae JJ. 2016. Pyrin inflammasome activation and
805 RhoA signaling in the autoinflammatory diseases FMF and HIDS. Nat Immunol 17:914-
806 21.
807 34. Park YH, Remmers EF, Lee W, Ombrello AK, Chung LK, Shilei Z, Stone DL, Ivanov MI,
808 Loeven NA, Barron KS, Hoffmann P, Nehrebecky M, Akkaya-Ulum YZ, Sag E, Balci-
809 Peynircioglu B, Aksentijevich I, Gul A, Rotimi CN, Chen H, Bliska JB, Ozen S, Kastner
810 DL, Shriner D, Chae JJ. 2020. Ancient familial Mediterranean fever mutations in human
811 pyrin and resistance to Yersinia pestis. Nat Immunol doi:10.1038/s41590-020-0705-6.
812 35. Masters SL, Lagou V, Jeru I, Baker PJ, Van Eyck L, Parry DA, Lawless D, De Nardo D,
813 Garcia-Perez JE, Dagley LF, Holley CL, Dooley J, Moghaddas F, Pasciuto E, Jeandel
814 PY, Sciot R, Lyras D, Webb AI, Nicholson SE, De Somer L, van Nieuwenhove E, Ruuth-
815 Praz J, Copin B, Cochet E, Medlej-Hashim M, Megarbane A, Schroder K, Savic S, Goris
816 A, Amselem S, Wouters C, Liston A. 2016. Familial autoinflammation with neutrophilic
817 dermatosis reveals a regulatory mechanism of pyrin activation. Sci Transl Med
818 8:332ra45.

819 36. McCoy MW, Marre ML, Lesser CF, Mecsas J. 2010. The C-terminal tail of Yersinia
820 pseudotuberculosis YopM is critical for interacting with RSK1 and for virulence. Infect
821 Immun 78:2584-98.
822 37. Jamilloux Y, Magnotti F, Belot A, Henry T. 2018. The pyrin inflammasome: from sensing
823 RhoA GTPases-inhibiting toxins to triggering autoinflammatory syndromes. Pathogens
824 and disease 76:fty020.
825 38. Magnotti F, Lefeuvre L, Benezech S, Malsot T, Waeckel L, Martin A, Kerever S, Chirita
826 D, Desjonqueres M, Duquesne A, Gerfaud-Valentin M, Laurent A, Seve P, Popoff MR,
827 Walzer T, Belot A, Jamilloux Y, Henry T. 2019. Pyrin dephosphorylation is sufficient to
828 trigger inflammasome activation in familial Mediterranean fever patients. EMBO Mol Med
829 11:e10547.
830 39. Nasa I, Kettenbach AN. 2018. Coordination of Protein Kinase and Phosphoprotein
831 Phosphatase Activities in Mitosis. Front Cell Dev Biol 6:30.
832 40. Aktories K. 2011. Bacterial protein toxins that modify host regulatory GTPases. Nat Rev
833 Microbiol 9:487-98.
834 41. Namboodiripad AN, Jennings ML. 1996. Permeability characteristics of erythrocyte
835 membrane to okadaic acid and calyculin A. American Journal of Physiology-Cell
836 Physiology 270:C449-C456.
837 42. Stutz A, Kolbe CC, Stahl R, Horvath GL, Franklin BS, van Ray O, Brinkschulte R, Geyer
838 M, Meissner F, Latz E. 2017. NLRP3 inflammasome assembly is regulated by
839 phosphorylation of the pyrin domain. J Exp Med 214:1725-1736.
840 43. Gavrilin MA, Abdelaziz DH, Mostafa M, Abdulrahman BA, Grandhi J, Akhter A, Abu
841 Khweek A, Aubert DF, Valvano MA, Wewers MD, Amer AO. 2012. Activation of the pyrin
842 inflammasome by intracellular Burkholderia cenocepacia. J Immunol 188:3469-77.
843 44. Wittig I, Braun HP, Schagger H. 2006. Blue native PAGE. Nat Protoc 1:418-28.
844 45. Kofoed EM, Vance RE. 2013. Blue native polyacrylamide gel electrophoresis to monitor
845 inflammasome assembly and composition. Methods Mol Biol 1040:169-83.
846 46. Choy MS, Swingle M, D'Arcy B, Abney K, Rusin SF, Kettenbach AN, Page R, Honkanen
847 RE, Peti W. 2017. PP1: Tautomycetin complex reveals a path toward the development
848 of PP1-specific inhibitors. Journal of the American Chemical Society 139:17703-17706.
849 47. Mitsuhashi S, Matsuura N, Ubukata M, Oikawa H, Shima H, Kikuchi K. 2001.
850 Tautomycetin is a novel and specific inhibitor of serine/threonine protein phosphatase
851 type 1, PP1. Biochemical and biophysical research communications 287:328-331.

852 48. Kreienbuhl P, Keller H, Niggli V. 1992. Protein phosphatase inhibitors okadaic acid and
853 calyculin A alter cell shape and F-actin distribution and inhibit stimulus-dependent
854 increases in cytoskeletal actin of human neutrophils.
855 49. Swingle M, Ni L, Honkanen RE. 2007. Small-molecule inhibitors of Ser/Thr protein
856 phosphatases, p 23-38, Protein Phosphatase Protocols. Springer.
857 50. Shi Y. 2009. Serine/threonine phosphatases: mechanism through structure. Cell
858 139:468-484.
859 51. Luheshi NM, Giles JA, Lopez-Castejon G, Brough D. 2012. Sphingosine regulates the
860 NLRP3-inflammasome and IL-1β release from macrophages. European journal of
861 immunology 42:716-725.
862 52. Jeru I, Papin S, L'Hoste S, Duquesnoy P, Cazeneuve C, Camonis J, Amselem S. 2005.
863 Interaction of pyrin with 14.3.3 in an isoform-specific and phosphorylation-dependent
864 manner regulates its translocation to the nucleus. Arthritis Rheum 52:1848-57.
865 53. Evdokimov AG, Anderson DE, Routzahn KM, Waugh DS. 2001. Unusual molecular
866 architecture of the Yersinia pestis cytotoxin YopM: a leucine-rich repeat protein with the
867 shortest repeating unit. J Mol Biol 312:807-21.
868 54. MacKintosh C, Beattie KA, Klumpp S, Cohen P, Codd GA. 1990. Cyanobacterial
869 microcystin-LR is a potent and specific inhibitor of protein phosphatases 1 and 2A from
870 both mammals and higher plants. FEBS letters 264:187-192.
871 55. Mao L, Kitani A, Hiejima E, Montgomery-Recht K, Zhou W, Fuss I, Wiestner A, Strober
872 W. 2020. Bruton tyrosine kinase deficiency augments NLRP3 inflammasome activation
873 and causes IL-1β–mediated colitis. The Journal of clinical investigation 130:1793-1807.
874 56. Simonet M, Falkow S. 1992. Invasin expression in *Yersinia pseudotuberculosis*. Infect
875 Immun 60:4414-4417.
876 57. McPhee JB, Mena P, Bliska JB. 2010. Delineation of regions of the Yersinia YopM
877 protein required for interaction with the RSK1 and PRK2 host kinases and their
878 requirement for interleukin-10 production and virulence. Infect Immun 78:3529-39.
879 58. Chung LK, Philip NH, Schmidt VA, Koller A, Strowig T, Flavell RA, Brodsky IE, Bliska JB.
880 2014. IQGAP1 is important for activation of caspase-1 in macrophages and is targeted
881 by Yersinia pestis type III effector YopM. MBio 5:e01402-14.
882 59. Loeven NA, Perault AI, Cotter PA, Hodges CA, Schwartzman JD, Hampton TH, Bliska
883 JB. 2021. The Burkholderia cenocepacia Type VI Secretion System Effector TecA Is a
884 Virulence Factor in Mouse Models of Lung Infection. mBio 12:e0209821.

885 60. Chae JJ, Komarow HD, Cheng J, Wood G, Raben N, Liu PP, Kastner DL. 2003.
886 Targeted disruption of pyrin, the FMF protein, causes heightened sensitivity to endotoxin
887 and a defect in macrophage apoptosis. Mol Cell 11:591-604.
888